Massresolved multiphoton ionization spectroscopy of jetcooled Cl2. I. Boundfreebound spectroscopy

Mohamed S. N. AlKahali, Robert J. Donovan, Kenneth P. Lawley, Zhiyuan Min, and Trevor Ridley

Mass-resolved multiphoton ionization spectroscopy of jet-cooled Cl$_2$. I. Bound-free-bound spectroscopy

Mohamed S. N. Al-Kahali, Robert J. Donovan, Kenneth P. Lawley, Zhiyuan Min, and Trevor Ridley
Department of Chemistry, The University of Edinburgh, West Mains Road, Edinburgh EH9 3JJ, Scotland

Spectroscopic constants, obtained using two-color optical double resonance *via* repulsive intermediate states, are presented for four ion-pair states of Cl$_2$; i.e., the $E(0_g^+)$, $\beta(1_g)$, $f(0_g^+)$, and $G(1_g)$ states. One-color excitation, also *via* a repulsive intermediate state, has been used to further extend the vibrational data for the $\beta(1_g)$ state. The same pumping scheme has been used to extend a vibrational progression in the $[^2\Pi_{1/2}]_c 4s; 1_g$ Rydberg state. The absence of perturbations when the $[^2\Pi_{1/2}]_c 4s; 1_g)$ Rydberg and the $\beta(1_g)$ ion-pair states cross, together with the key role played by the intermediate $C(1_u)$ state in accessing both singlet and triplet final states, are discussed in terms of the changes in spin–orbital coupling schemes that are required on bond stretching. © *1996 American Institute of Physics.* [S0021-9606(96)01605-X]

I. INTRODUCTION

Recent results have revealed how continuum states can be used as intermediates in both (1+1) and (1+2) optical double resonance excitation of the ion-pair states of I$_2$ and Cl$_2$.[1–4] Some degree of bond stretching is involved and appreciable intensity is observed when both pump and probe steps have large transition dipole moments. In addition, the wavelength of the probe photon (λ_{probe}) must lie to shorter wavelengths than the red extremum of the final to intermediate state emission system. The ability to extend the vibrational progression of the $G'(1_g)$ ion-pair state of Cl$_2$, which dissociates to Cl$^+$($^1D_2$)+Cl$^-$($^1S_0$), shows how the technique is particularly useful for accessing high-lying vibronic states.[4] Furthermore, good quality rotational data can be obtained without a prior rotational analysis of the intermediate state or tuning to a resonant intermediate state.

RKR data below 63 000 cm^{-1} for all six *gerade* ion-pair states of Cl$_2$ which dissociate to Cl$^+$($^3P_{(2,1,0)}$)+Cl$^-$($^1S_0$) have been previously obtained from optical–optical double resonance (OODR) studies *via* the bound levels of the $B(^3\Pi_{0u}^+)$ and $A(^3\Pi_{1u})$ states.[5–10] In the present work we use OODR *via* these same states *above their dissociation limits* as well as *via* the purely repulsive $C(^1\Pi_{1u})$ state, to access four of the six *gerade* ion-pair states up to energies of 72 000 cm^{-1}.

It has been predicted theoretically that strong interactions should take place between some of the ion-pair states based on Cl$^+$(^3P_J) and low-lying Rydberg states in the region above 70 000 cm^{-1}.[11] In particular, it was proposed that the crossing of the inner wall of the $^3\Pi_g$ ion-pair states with the outer wall of the triplet 4s Rydberg states would result in double-minimum potentials. Li *et al.*[12] suggested that results from their mass-resolved one-color (2+1) resonance-enhanced multiphoton ionization (REMPI) studies supported this theory. Their spectra contained a long vibrational progression of red-degraded bands between 70 000 and 74 000 cm^{-1}, provisionally assigned as having 1_g symmetry, with spacings indicative of an ion-pair state based on Cl$^+$(^3P_J) (i.e., one from the first cluster). Our current OODR results

confirm their assignment, extend their data and give the absolute vibrational numbering. It was further proposed[12] that only those red-degraded bands above the barrier of the double-minimum potential were observed. In the present paper we reinvestigate the region of this proposed avoided crossing in the light of the OODR and REMPI data which extend up to 78 000 cm^{-1}. (In this paper we use the terms REMPI and OODR to refer to one- and two-color experiments respectively.) Efficient rotational cooling, isotopic separation and accurate measurements of band positions mean that any vibrational shifts resulting from ion-pair/Rydberg interactions can be identified. The role of the $C(^1\Pi_{1u})$ state, resonant at the one-photon level, in the appearance of the ion-pair progression is discussed.

Previous REMPI spectra[12,13] have shown a second very unusual feature in the energy range 64 000–74 000 cm^{-1}. Transitions are seen from $v''=0$ of the ground state to $v'=0$–15 of the $[^2\Pi_{1/2}]_c 4s; 1_g$ Rydberg state. Typically, Franck–Condon factors dictate that vertical transitions from the ground state will only access $v'=0$–4 of the unperturbed Rydberg state to any appreciable extent. The extended progression seen following two-photon excitation contrasts with the results of electron energy loss studies[14] where only $v'=0$–6 bands were observed, with an intensity maximum at $v'=2$. It was concluded[12] that the unusual two-photon behavior was again due to the C state, present at the one-photon level, causing some bond stretching in the overall two-photon transition. The criteria necessary for the observation of transitions *via* a repulsive intermediate state[2] which result in bond stretching are applied here in the analysis of the $[^2\Pi_{1/2}]_c 4s; 1_g$ Rydberg state.

II. EXPERIMENT

The molecular beam was generated by pulsing a mixture of Cl$_2$ and He through a General Valve nozzle with a 250 μm diameter aperture into the ionization region of a linear time-of-flight mass spectrometer. Ions were collected at 90° to both the molecular and laser beams. Mass-resolved ion sig-

nals were processed by a Stanford Research SR250 boxcar integrator and stored on a personal computer. $^{35}Cl_2$ spectra were recorded by collecting $^{35}Cl^+$ ions and subsequently subtracting the simultaneously recorded $^{37}Cl^+$ spectrum.[3] For the vibrational data, a mixture of 150 torr of Cl_2 and 450 torr of He was used while for the rotational data, where less efficient rotational cooling was required, the mixture was 150 torr of Cl_2 and 150 torr of He.

In the OODR experiments the molecular beam was crossed at 90° by two counterpropagating laser beams. These were generated by a Lambda Physik EMG 201MSC excimer laser which simultaneously pumped two Lambda Physik dye lasers; an FL3002E (pump) and an FL2002E (probe). The fixed probe photons, between 225 and 250 nm, of ca. 1 mJ per pulse were produced by frequency doubling the output of the dyes Coumarin 2, Coumarin 47, and Coumarin 102. The fundamentals of the dyes Coumarin 47, Coumarin 120, Stilbene 3, Furan 2, PBBO, QUI, DMQ, and PTP were used in the pump laser. In order to obtain photons which were parallel or perpendicular to the probe photons, the pump beam was passed through a linear polarizer (Lambda Physik FL50) and then through a double Fresnel rhomb. The lasers were directed *via* 5 cm focal length lenses into the molecular beam. Both lenses were focused outside of the ionization region in order to minimize one-color ion signals. The rotational data were recorded with intracavity etalons in both lasers. The vibrational spectra were calibrated in two stages. Firstly, λ_{probe} was chosen such that the dye fundamental, before frequency doubling, excited an optogalvanic line of neon. The scanned λ_{pump} was then also calibrated by neon optogalvanic lines.

In the one-color (2+1) REMPI experiments, ions were excited by the fully focussed, frequency doubled outputs of the dyes Rhodamine B, Coumarin 153, and Coumarin 307. Dye laser fundamental wavelengths above 500 nm were calibrated against the $I_2(B-X)$ spectrum.

III. RESULTS

A. OODR studies of the ion-pair states

OODR spectra of the $E0_g^+(^3P_2)$, $f0_g^+(^3P_0)$, $\beta1_g(^3P_2)$, and $G1_g(^3P_1)$ ion-pair states of jet-cooled Cl_2 have been recorded following excitation *via* unbound intermediate states. Three fixed λ_{probe} values of 250, 230, and 225 nm were used together with a tunable pump beam. The two-photon energy range covered was 61 000–72 000 cm^{-1}. The OODR spectrum of Cl_2 between 61 000 and 69 400 cm^{-1}, shown in Fig. 1, was recorded by scanning λ_{pump} from 340 to 480 nm with λ_{probe} fixed at 250 nm. It was shown in a previous paper that the overall intensities of the 0_g^+ state bands are enhanced relative to those of the 1_g state bands when the linearly polarized pump and probe photons are parallel rather than perpendicular to each other. Thus the spectrum in Fig. 1 was recorded with parallel polarization.

The spectrum is normalized to the power of the pump photons. However, the relative intensities of the bands in the upper and lower traces of Fig. 1 require further comment. There is a loss of intensity in all progressions around 64 000
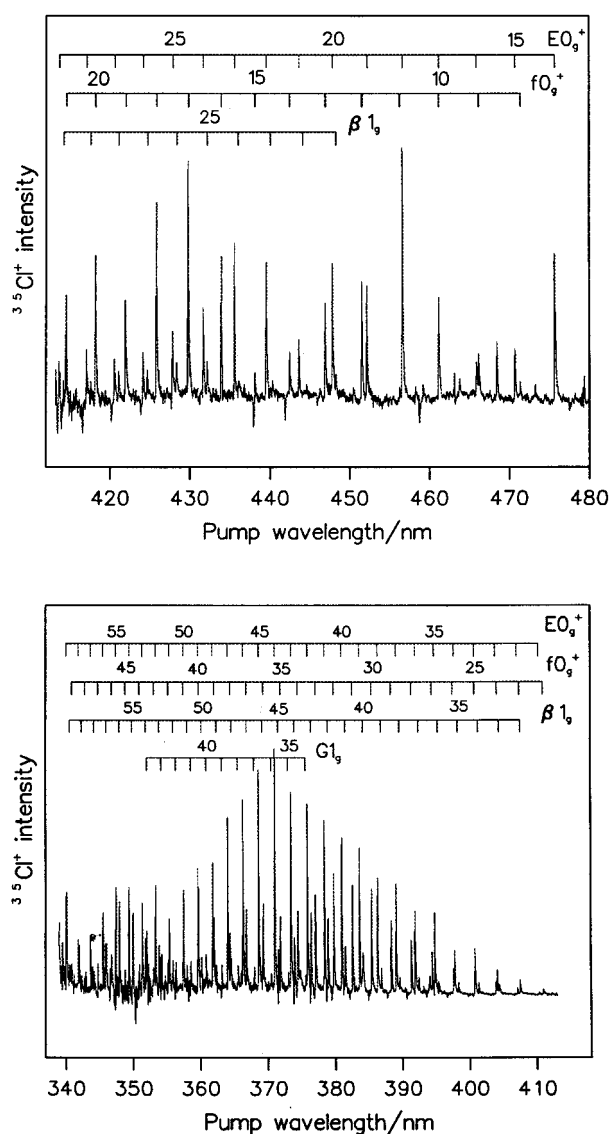

FIG. 1. The bound-free-bound OODR spectrum of jet-cooled $^{35}Cl_2$ between 61 000 and 69 400 cm^{-1}. λ_{probe} was fixed at 250 nm and λ_{pump} was scanned between 480 and 340 nm.

cm^{-1} (λ_{pump}=415 nm in Fig. 1) and it is difficult to follow the intensity pattern through this region. Thus the intensity of the upper trace relative to that of the lower may not be exactly comparable. Furthermore, in this spectrum one additional probe photon has sufficient energy to reach the first molecular ionization potential, but the probe beam has only low power and so ionization by this route may not be very efficient. For λ_{pump} less than 380 nm, one additional pump photon is sufficient to reach the ionization potential and so the extra power of the pump photons may distort the intensity profiles below 380 nm.

Between 340 and 480 nm, the pump photon excites at least two valence states, namely the $B(^3\Pi_{0u}^+)$ state, above its dissociation limit, and the purely repulsive $C(^1\Pi_{1u})$ state.[15] Absorption to the $A(^3\Pi_{1u})$ state above its dissociation limit has not been reported, although the bound region of the
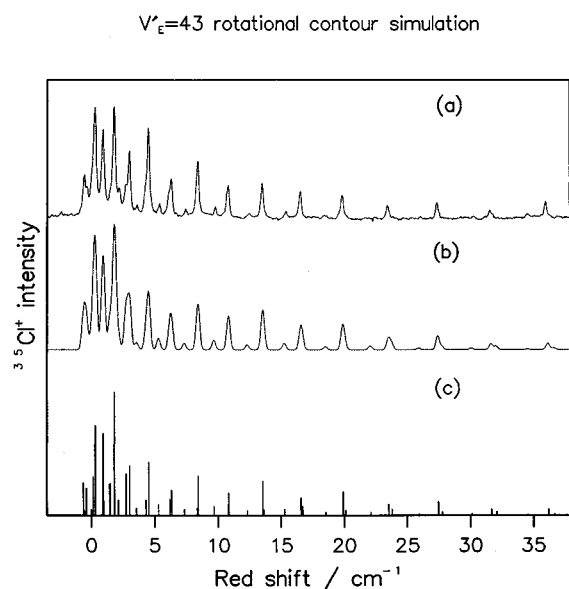
V'ₑ=43 rotational contour simulation

FIG. 2. The rotational contour of the $E0_g^+(^3P_2)$ state (43,0) band: (a) experimental, recorded with parallel polarization, (b) simulation, and (c) individual O, Q, and S branches. The rotational population was simulated by a two-temperature dependence described by the equation given in Ref. 4, where T_1 and T_2 are 2.5 and 20 K, respectively.

FIG. 3. The (2+1) REMPI spectrum of jet-cooled $^{35}Cl_2$ between 69 500 and 78 000 cm⁻¹ normalized to the laser power.

$A(^3\Pi_{1u})$ state has been well characterized.[16] From a splined extension of the inner wall of the potential it is estimated that $A \leftarrow X(^1\Sigma_g^+)$ absorption should extend down to 350 nm with a maximum at 410 nm.

The strongest bands seen in spectra recorded *via* the $B(0_u^+)$ state should be those terminating on the $E(0_g^+)$ and $f(0_g^+)$ ion-pair states according to the $\Delta\Omega=0$ propensity rule for valence to ion-pair state transitions. Low vibrational levels of both states have been characterized in OODR studies *via* bound levels of the $B(0_u^+)$ state by Ishiwata *et al.*[5,6] Dispersed emission spectra showed that the $E \rightarrow B$ and $f \rightarrow B$ systems have red extrema at 259 and 250 nm, respectively. Thus a λ_{probe} of 250 nm should be effective in exciting the reverse transitions from the unbound region of the $B(0_u^+)$ state. Strong transitions to $E(0_g^+)$ and $f(0_g^+)$ state vibrational levels are indeed observed beginning at $\lambda_{pump}=480$ nm. The lowest observed levels overlap the previous vibrational data[5,6] with excellent agreement making assignment unambiguous.

The $\beta(1_g)$ state is also identified from an overlap with previous vibrational data.[7] When λ_{pump} is ≥ 400 nm, the $\beta(1_g)$ state is excited chiefly by $\beta \leftarrow A \leftarrow X$ transitions while $\beta \leftarrow C \leftarrow X$ transitions dominate when λ_{pump} is ≤ 400 nm. Identification of the fourth progression follows from the fact that its vibrational levels run very nearly parallel with those of the $f(0_g^+)$ state. Of the three remaining *gerade* states, the $G1_g(^3P_1)$, $D'2_g(^3P_2)$, and $0_g^-(^3P_0)$, only the levels of the $G(1_g)$ state follow this trend at low v'.[5,7,8,10] Furthermore, the levels shown in Fig. 1 are entirely consistent with extrapolation of the $G(1_g)$ state vibrational data.[10]

Figure 2(a) shows a typical ion-pair state rotational contour: the (43,0) band of the $E(0_g^+)$ state progression was
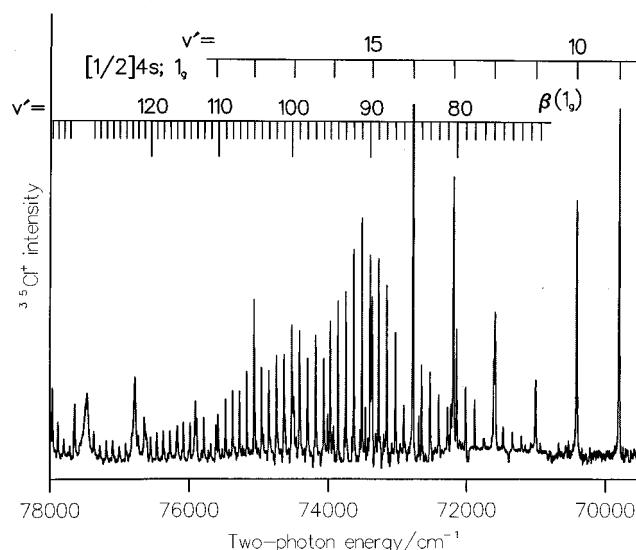
recorded with parallel polarization and intracavity etalons in both lasers. The observed linewidths (0.2 cm⁻¹) are larger than expected from the two laser linewidths (each 0.04 cm⁻¹), probably because of power and/or Doppler broadening. However, reasonably accurate rotational constants can still be obtained from simulations of the line positions using the appropriate Hönl–London factors.[4] An example is shown, together with a stick diagram, indicating the individual rotational line positions and intensities [Figs. 2(b) and 2(c)]. In this way eight B_v values for each electronic state were obtained in the ranges: $v'=43-59(E)$, $v'=29-62(f)$, and $v'=41-69(\beta)$. The $G(1_g)$ state bands are too weak to obtain reliable B_v values.

There is a significant difference (ca. 1.5 cm⁻¹) between the band maxima of the $E(0_g^+)$ and $f(0_g^+)$ states measured in the present work and the band origins reported previously.[5,6] Rotational contour simulations have shown that when perpendicularly polarized photons are used a relatively strong O branch head appears ca. 1.5 cm⁻¹ to the blue of the band origin. This bandhead forms the observed band maximum. In view of this, 1.5 cm⁻¹ was subtracted from the observed $E(0_g^+)$ and $f(0_g^+)$ state band positions. The $\beta(1_g)$ state bands do not show an equivalent discrepancy because the different relative strengths of the branches do not shift the band maximum from the origin under low resolution conditions.

The vibrational levels of all four states obtained in the present work, accurate to ± 0.5 cm⁻¹, were combined with levels generated from the appropriate published data and fitted to conventional Dunham expansions. The B_v values were treated similarly to give the rotational constants. Only values for the $^{35}Cl_2$ isotopomer were included. The derived molecular constants are presented in Table I.

B. (2+1) REMPI studies of the ion-pair states

Figure 3 shows the (2+1) REMPI spectrum of jet-cooled

TABLE I. Molecular constants for the $E(0_g^+)$, $\beta(1_g)$, $f(0_g^+)$, and $G(1_g)$ ion-pair states of $^{35}Cl_2$. The molecular constants are valid up to v': (a) 74, (b) 120, (c) 63, (d) 44, (e) 59, (f) 69, and (g) 62. All values are in cm^{-1} and the numbers in parenthesis are equivalent to one standard deviation.

	$E(0_g^+)$ (a)	$\beta(1_g)$ (b)	$f(0_g^+)$ (c)	$G(1_g)$ (d)
$Y_{0,0}$	57 819.71(26)	57 571.73(37)	59 356.45(24)	59 295.90(19)
$Y_{1,0}$	251.851(49)	252.455(88)	256.832(53)	256.558(40)
$Y_{2,0}$	−1.0303(28)	−1.0398(66)	−1.1936(34)	−1.1949(21)
$Y_{3,0}$ (10^{-3})	2.483(60)	3.12(22)	3.868(80)	3.357(33)
$Y_{4,0}$ (10^{-5})	−0.296(40)	−1.40(32)	−0.698(64)	
$Y_{5,0}$ (10^{-8})		8.3(23)		
$Y_{6,0}$ (10^{-10})		−2.22(64)		
	(e)	(f)	(g)	
$Y_{0,1}$	0.116 32(28)	0.114 54(31)	0.116 33(22)	
$Y_{1,1}$ (10^{-4})	−6.31(36)	−6.25(17)	−6.90(28)	
$Y_{2,1}$ (10^{-6})	1.09(57)	1.07(22)	1.26(44)	

$^{35}Cl_2$, recorded on the $^{35}Cl^+$ mass channel, between 70 000 and 78 000 cm^{-1} which corresponds to one-photon wavelengths of 285.7 and 256.4 nm. For reasons which will be explained in the section on Rydberg states, the spectrum is normalized to the laser power and not to the square of the laser power.

The ion-pair progression observed in Fig. 3 was previously assigned[12] as arising from the $\beta(1_g)$ state. This assignment can now be confirmed from the current OODR results which overlap both the earlier low v' data and the REMPI data. Thus not only the symmetry but also the numbering of the vibrational levels therein are established, i.e., the bands first observed by Li *et al.*[12] correspond to $v'=65$–94 of the $\beta(1_g)$ state. The present studies extend v' up to 120. Over this range the levels are essentially unperturbed within the limits of the accuracy of the measurement procedures, i.e., ±0.5 cm^{-1} for the OODR data and ±2 cm^{-1} for the REMPI data. The REMPI data values were also included in the Dunham expansion defined by the constants listed in Table I.

C. (2+1) REMPI studies of the Rydberg states

The (2+1) REMPI spectrum of jet-cooled $^{35}Cl_2$ and $^{35}Cl^{37}Cl$, recorded on the $^{35}Cl^+$ mass channel, between 63 000 and 67 000 cm^{-1} is shown in Fig. 4. With the exception of the most intense band at 65 300 cm^{-1}, where the molecular ion forms <5% of the total ion signal, only atomic ion signals were observed. The strong progression is due to the $[^2\Pi_{1/2}]_c 4s$; 1_g Rydberg state. Isotopic shifts confirm the previous assignment[12,13] of the origin at 64 026 cm^{-1}. Vibrational levels up to $v'=19$ were observed (see also Fig. 3) and the transition wavenumbers for the $^{35}Cl_2$ isotopomer are given in Table II. These values are in reasonable agreement with previous measurements[12] as can be seen from Table II.

Previously, no attempt had been made to power normalize the spectrum although it was noted[12] that the $v'=2$ band was the most intense. With this aim in mind we have measured the power dependence of the $v'=1$, 2, and 4 bands. All three have intensities which increase linearly with laser power and the spectra in Figs. 3 and 4 are normalized ac-

cordingly. This behavior contrasts markedly with that of the $5s$, $6s$, and $7s$ Rydberg states[17] which have a power-squared dependency. The latter behavior is what is expected for a strictly coherent two-photon absorption *via* virtual intermediate states.

Figure 4 illustrates the large intensity of the (2,0) band relative to other members of the progression. Irregular intensities such as these are one indication of an interaction with a second electronic state. However, in contrast to the widely varying intensities, the vibrational spacings are fairly regular. Only the $v'=1$ level is slightly shifted and this by only -7 cm^{-1}. Theoretical calculations[11] predict that this Rydberg state (labeled $^1\Pi_g 4s$) should be crossed near to its origin by a repulsive $^1\Pi_{1g}$ valence state. Further evidence for this crossing can be gained from a consideration of the bandwidths of the vibronic levels. In this $4s$ Rydberg state they are ca. 15 cm^{-1} while for the $5s$ and $6s$ states, under the
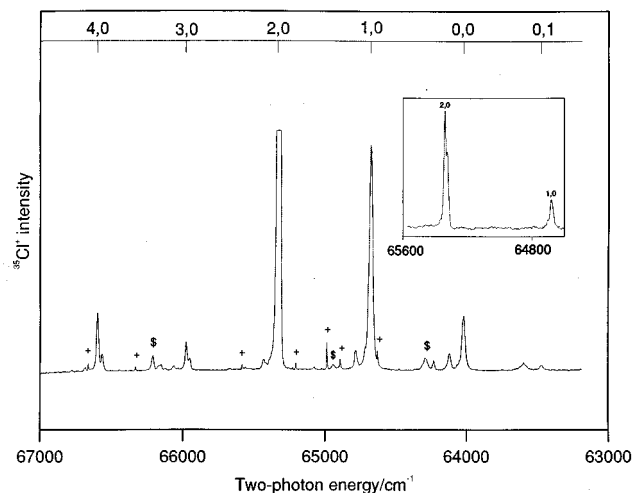
FIG. 4. The (2+1) REMPI spectrum of jet-cooled $^{35}Cl_2$ and $^{35}Cl^{37}Cl$ between 63 000 and 67 000 cm^{-1}, normalized to the laser power, showing the $[^2\Pi_{1/2}]_c 4s$; 1_g state progression. The inset illustrates the relative strengths of the (1,0) and (2,0) bands. $'s indicate the (2,0), (3,0), and (5,0) bands of a $[^2\Pi_{3/2}]_c 4s$ state progression and the +'s are (2+1) lines of atomic Cl.

TABLE II. Observed band positions of the $[^2\Pi_{1/2}]_c 4s; 1_g$ Rydberg state of ^{35}Cl$_2$. Literature values come from Ref. 12.

v'	$\nu_{obs.}$ (cm^{-1})	$\nu_{lit.}$ (cm^{-1})	v'	$\nu_{obs.}$ (cm^{-1})	$\nu_{lit.}$ (cm^{-1})
0	64026	64027	10	70391	70392
1	64678	64681	11	70995	70998
2	65340	65332	12	71593	71600
3	65992	65986	13	72183	72187
4	66637	66640	14	72775	72771
5		67270	15	73353	73343
6		67905	16	73925	
7		68534	17	74492	
8	69165	69220	18	75063	
9	69782	69779	19	75609	

same experimental conditions, they are only ca. 3 cm^{-1}.[17] These results are indicative of the lifetime of the $4s$ Rydberg state being very much shortened by predissociation following interaction with a repulsive state. Thus it is concluded that the $[^2\Pi_{1/2}]_c 4s$; 1_g state is crossed on its inner or outer wall (between $v'=1$ and $v'=2$), by a $^1\Pi_{1g}$ repulsive valence state with which it interacts weakly. The increased intensities of the (1,0) and (2,0) bands are almost certainly a consequence of an increase in the efficiency of the ionization step. In the (1,0) and (2,0) bands the ion signal results from ionization of Cl atoms, formed from the predissociation of the Rydberg levels, which is probably more efficient than ionization of the Rydberg state itself.

Two bands at 64 290 and 66 233 cm^{-1}, not belonging to the major $4s$ progression, have been observed previously and assigned from isotopic shifts and photoelectron data[12,13] as the (2,0) and (5,0) bands of a second progression due to a state with a $[^2\Pi_{3/2}]_g$ ionic core. A third weak band assignable to the (3,0) band at 64 942 cm^{-1} is observed in the present studies, further supporting this assignment. Extrapolation of the three values predicts a (0,0) band at 62 970 cm^{-1}. There is not enough evidence to unambiguously determine to which of the 2_g or 1_g components of the $[^2\Pi_{3/2}]_c 4s$ Rydberg state this origin belongs. It is proposed that the (2,0) and (3,0) bands gain their intensity through interaction with a $^3\Pi_g$ repulsive state *via* the same mechanism as the $[^2\Pi_{1/2}]_c 4s$; 1_g state. This interaction and the singlet equivalent discussed above have been predicted by Peyerimhoff and Buenker.[11]

The $^3\Pi_g$ Rydberg state reported by Li *et al.*[12] is not observed. The weak bands to the blue of each of the $[^2\Pi_{1/2}]_c 4s$; 1_g state bands are all consistent within ± 2 cm^{-1} with being hot bands of that progression. Isotopic shifts also support this assignment. The (3+1) REMPI lines of atomic chlorine, labeled in Fig. 4, agree with the literature values[18] to within ± 2 cm^{-1}.

IV. DISCUSSION

A. Potential energy curves

Potential energy curves of all of the electronic states discussed in the present paper are illustrated in Fig. 5. The $E0_g^+(^3P_2)$ and $f0_g^+(^3P_0)$ state potentials were generated by

an RKR treatment of the molecular constants summarized in Table II. The method of producing the $\beta 1_g(^3P_2)$ state potential has been described in detail elsewhere.[3] Briefly, the outer limb at $R>6$ Å, corresponding to an energy of ca. 75 000 cm^{-1}, is described by a truncated Rittner potential of the form

$$V(R) = D_e - C_1/R - C_4/R^4 - C_6/R^6, \qquad (1)$$

where C_1 is the Coulombic term, C_4 is the polarization coefficient, and C_6 represents the effect of dispersion forces. A trial spline function for the inner wall of the potential is then defined by knot points positioned to join the splined portion smoothly onto the RKR turning points of the potential minimum, which span the range $2.45<R$ (Å)<3.65. A similar number of knot points is used to join the outer branch of the RKR potential to the asymptotic form in Eq. (1). The knot points are adjusted until the potential reproduces the observed spacings and absolute positions of the vibrational levels to within ± 3 cm^{-1} over the range 57 000–78 000 cm^{-1}. The knot points are given in Table III.
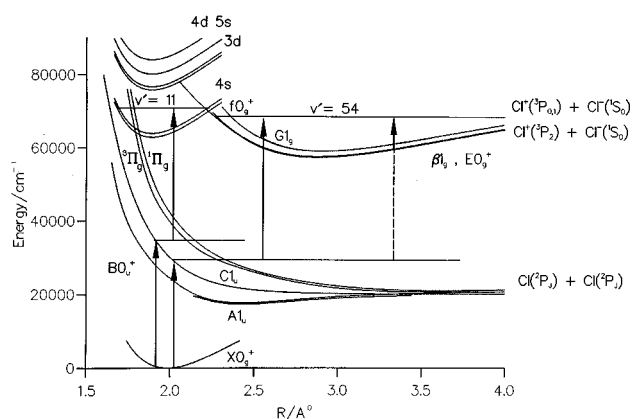
FIG. 5. Potential energy curves of Cl$_2$ discussed in this paper. The arrows illustrate two excitation pathways *via* the $C(^1\Pi_{1u})$ state which involve bond stretching with the conservation of nuclear kinetic energy. The one-color REMPI scheme excites $v'=11$ of the $[^2\Pi_{1/2}]_c 4s$; 1_g Rydberg state and the two-color OODR scheme excites $v'=54$ of the $\beta(1_g)$ ion-pair state. It can be seen that for a particular $C\leftarrow X$ transition there are two $\beta \leftarrow C$ transitions which occur with the conservation of kinetic energy.

TABLE III. Knot points used to describe the $\beta(1_g)$ ion-pair state potential.

R (Å)	V (cm^{-1})	R (Å)	V (cm^{-1})
2.00	81 356.9	3.40	60 296.5
2.10	75 697.8	3.50	61 104.9
2.20	71 228.6	3.60	61 933.2
2.30	67 181.2	3.70	62 773.3
2.40	63 746.7	3.80	63 618.0
2.50	61 044.0	3.90	64 451.4
2.60	59 249.1	4.00	65 264.5
2.70	58 183.3	4.50	68 942.2
2.80	57 674.0	5.00	71 908.7
2.876	57 572.6	5.50	74 317.0
2.90	57 582.3	6.00	76 268.9
3.00	57 798.1	6.50	77 794.5
3.10	58 235.5	7.00	79 096.2
3.20	58 829.0	7.50	80 220.4
3.30	59 528.5	8.00	81 201.8

FIG. 6. Simulation of the $\beta \rightarrow C$ emission from $v'=70$ showing a red extremum at 280 nm.

Koenders *et al.*[13] simulated the bandhead contours of the (2,0) and (5,0) bands of the $[^2\Pi_{1/2}]_c4s; 1_g$ Rydberg state in the (2+1) REMPI spectrum of Cl_2. B_v values were obtained, from which α_e, B_e, and R_e were estimated. The R_e value obtained, 1.84 Å, is very small compared to those of the ground state of the ion, 1.89 Å, and the molecular ground state, 1.99 Å. We have shown in the present work that the 2,0 band is perturbed and this must place some uncertainty on the extrapolated α_e and R_e values. In the absence of any other information on the Rydberg potentials, all of those in Fig. 5 are represented instead by the ground state of the ion.[19]

The $X(^1\Sigma_g^+)$, $B(^3\Pi_{0u}^+)$, and $C(^1\Pi_{1u})$ states are generated from data given in the literature.[20–22] The repulsive $^3\Pi_g$ and $^1\Pi_g$ valence state potentials are generated from a series of knot points placed so that they cross the $4s$ Rydberg states in positions estimated from the current experimental results and have the correct dissociation limits. The relative positions of the $4s$ Rydberg states and the $^{1,3}\Pi_g$ repulsive valence states shown in Fig. 5 agree well with those predicted from the calculations of Peyerimhoff and Buenker[11] although the absolute positions are all slightly offset.

B. Bond stretching in the (2+1) REMPI spectrum

The lowest energy two-photon transition to the $\beta(1_g)$ ion-pair state seen in Fig. 3 is the (71,0) band at 70 929 cm^{-1} (one-photon wavelength=282 nm). For this transition the inner turning point of the upper state is 2.20 Å, somewhat larger than the outer turning point of the lower state (2.05 Å). Despite the small Franck–Condon factors such weak transitions can sometimes be observed: for instance, $v'=6$ of the B state in Cl_2 ($R_{min}=2.20$ Å) can be excited from $v''=0$ of the X state.[20] Thus the spectrum observed in this region might be explained without having to invoke bond stretching. However, if the two-photon absorption to the $\beta(1_g)$ state is vertical the intensities of the bands should increase monotonically in line with the increase in the Franck–Condon factors as higher v' levels are accessed. The power normalized spectrum in Fig. 3 does not behave in this way. Al-
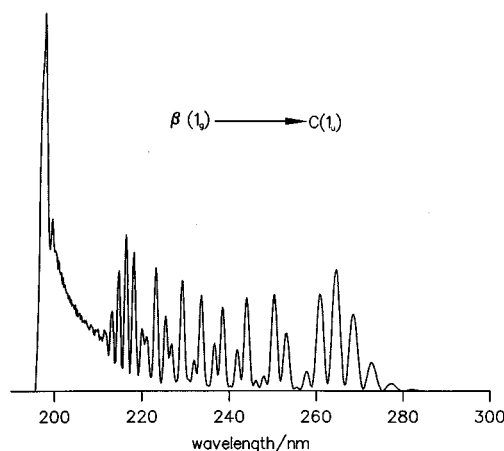
though the intensities increase with energy from 71 000 to 73 500 cm^{-1}, they then decrease to 78 000 cm^{-1}. Over this entire range the $\langle X|\beta \rangle$ Franck–Condon factors increase by a factor of ca. 10^4. In light of this, the role of bound-free-bound transitions and that of the $C(^1\Pi_{1u})$ state at the one-photon level, must be examined.

It was shown in the OODR (*two-color*) spectra that low levels of the $\beta(1_g)$ state can be accessed from the ground state *via* the $C(^1\Pi_{1u})$ state with some degree of bond stretching. We have shown previously that for efficient *one-color* excitation *via* repulsive intermediate states there are three criteria. Firstly, excitation to the intermediate state should be close to the absorption maximum. Secondly, and more importantly, excitation from the intermediate state that is undergoing bond stretching (dissociating) must be to the blue of, and preferably close to, the red extremum of the corresponding downward (i.e., reverse) bound-free fluorescence. Thirdly, both transitions should be fully allowed. Thus, with one-color excitation a window is defined by the overlap region for the two separate excitation steps. Knowing this, it becomes straightforward to account for the envelope of the $\beta(1_g)$ state bands in Fig. 3. Firstly, the high wavelength limit (λ_{max}) of the envelope is determined by the red extremum of the $\beta \rightarrow C$ emission system. A simulation of this system from $v'=70$, using the potentials in Fig. 5, is shown in Fig. 6. From this it can be seen that λ_{max} lies around 280 nm. Secondly, the low wavelength limit (λ_{min}) corresponds to the end of the $C \leftarrow X$ absorption which occurs at 260 nm.[15] The range 280–260 nm gives a two-photon energy range of 71 429–76 923 cm^{-1} which agrees well with the envelope of $\beta(1_g)$ state vibrational bands seen in Fig. 3. The present work parallels a previous study in which an equivalent one-color $E \leftarrow B \leftarrow X$ two-photon excitation spectrum of I_2 involving bond stretching was reported.[1] The $G 1_g(^3P_1) \leftarrow C \leftarrow X$ pathway is not available because the red extremum of the $G \rightarrow C$ emission lies at 260 nm,[10] i.e., there is little or no overlap with the $C \leftarrow X$ absorption.

The question now arises of how similar considerations

can be applied to the extended $[^2\Pi_{1/2}]_c 4s$; 1_g Rydberg progression. Two factors explain why this Rydberg state is seen much more strongly than any other $4s\Omega$ sub-state. Firstly, like the $X(^1\Sigma_g^+)$ and $C(^1\Pi_{1u})$ states, it is nominally a singlet or contains a large singlet component, the $[^2\Pi_{3/2}]4s1g$ state having predominantly triplet character. Secondly, the probe step is a favourable, parallel $1_u \rightarrow 1_g$ $(\sigma_u \rightarrow ns)$, transition. The potential minimum of the Rydberg state lies vertically above the steeply repulsive inner wall of the C state and so there is no maximum in the Mulliken difference potential between them and, hence, there is no fixed red extremum in the Rydberg$\rightarrow C$ emission as v' is scanned. Simulations of this emission system from various upper state levels indicate that any photon used in the current studies, i.e., 313–255 nm, can excite the reverse transition. The same $C \leftarrow X$ short wavelength limit of 260 nm that is observed in the ion-pair excitation also applies here. The range of v' levels of the Rydberg state that are observed, $v' = 0$–19, agrees with these predictions.

C. Electronic structure of the excited states of Cl$_2$

We will discuss the interpretation of just two aspects of the results presented above in terms of the electronic structure of the states involved. The first observation is that the $\beta(1_g)$ ion-pair state crosses the manifold of $[\omega_c]4s$ Rydberg states without appreciable perturbation of its vibrational progression. The second is that the $C(^1\Pi_{1u})$ state is an efficient gateway to the triplet $\beta(1_g)$ state.

Li *et al.*[12] proposed that, in their $(2+1)$ REMPI experiment, only ion-pair vibrational levels lying above the top of the barrier of the adiabatic double minimum state formed by the avoided crossing of the $\beta(1_g)$ ion-pair state with the $[3/2]4s\sigma$ Rydberg state were observed. The present results show that this is not the case and that the $\beta(1_g)$ ion-pair vibrational progression (nominally in the outer well in the adiabatic description) continues unperturbed through the region of the adiabatically avoided crossing. Such behavior points to a relatively small electronic coupling matrix element $\langle [3/2]_c 4s(1_g)|H|\beta(1_g)\rangle$ (i.e., with the Franck–Condon factor $\langle v(Ry)|v(\text{ion-pair})\rangle$ removed) in the diabatic description (probably less than 100 cm^{-1}). The reason for

this can be seen in the dominant electronic configurations of the two states.

The cluster of Ω states $[\omega_c]4s$, $\Omega = 2$, $1(2)$, 0 all have the configuration $[\sigma_g^2 \pi_u^4 \pi_g^3]4s$, with the two $\Omega = 1$ states being a mixture of $^3\Pi_{1g}$ and $^1\Pi_{1g}$ in Hund's case (a). The β state in I$_2$ has generally been given the configuration $\sigma_g^2 \pi_u^2 \pi_g^4 \sigma_u^2$; $^3\Sigma_{1g}^-$ [abbreviated to (2242)] (Ref. 23) on the grounds that this has a higher σ-bonding occupancy than the (1432) $^3\Pi_{1g}$ configuration, which is therefore assigned to the next highest 1_g ion-pair state, the G state. We will use the same configurations to describe the equivalent states in Cl$_2$. It is then clear that the β-state molecular orbital (MO) configuration differs from that of the $[\omega_c]4s$ Ω cluster by the assignment of more than two electrons and so the two configurations cannot be coupled by the two-electron repulsion terms $1/r_{ij}$ in the Hamiltonian (neither are they connected by the spin–orbit operator). Significant interactions have been predicted[11] between the triplet $4s$ Rydberg states and the $^3\Pi_g$ ion-pair states. The latter have the predominant configuration (1432) and are labeled $f0_g^+(^3P_0)$, $G1_g(^3P_1)$, $D'2_g(^3P_2)$, and $0_g^-(^3P_0)$ but none of the vibrational progressions of these states have been followed through the interaction region.

The role of the C state requires a more detailed examination of the way in which the electronic structures of states change with increasing bond length. The single-photon absorption spectrum of Cl$_2$ in the range 420–340 nm is dominated by the $C \leftarrow X$ continuum, with the $B \leftarrow X$ and $A \leftarrow X$ systems relatively weak compared with the heavier halogens. The C state in the range $R \approx 1.9$–2.1 Å is thus essentially the pure singlet state $^1\Pi_{1u}$, and the B state the triplet $^3\Pi_{0u}^+$, with a small amount of singlet character $(^1\Sigma_{0u}^+)$ induced by spin–orbit coupling. In single configuration terms, both these Π-states would be assigned (2431) at short interatomic distances. At large R, the valence states are most appropriately described in the $J_A M_A J_B M_B$ coupling scheme. Two 1_u states, the A and C, correlate with two ground state, Cl($^2P_{3/2}$), atoms.[24] Inspection of the atomic electronic structure in terms of $3p_0$, $3p_1$, and $3p_{-1}$ atomic orbital occupancy leads to the following projections onto the Hunds case (a) coupling scheme for these two 1_u states:

$$1_u(1); 1/\sqrt{2}[|^2P_{3/2,3/2}\rangle_A|^2P_{3/2,-1/2}\rangle_B + |^2P_{3/2,3/2}\rangle_B|^2P_{3/2,-1/2}\rangle_A]$$

$$\equiv 1/\sqrt{3}\{1/\sqrt{2}[^3\Pi_{1u}(1) + {}^1\Pi_{1u}(1)] + 1/\sqrt{2}[^3\Pi_{1u}(2) + {}^1\Pi_{1u}(2)] - {}^3\Sigma_{1u}(1)\},$$

$$1_u(2); \quad |^2P_{3/2,1/2}\rangle_A|^2P_{3/2,1/2}\rangle_B \equiv 1/\sqrt{7}\{2\,{}^3\Sigma_{1u}(2) + 1/\sqrt{2}[^3\Pi_{1u}(1) - {}^1\Pi_{1u}(1) + {}^3\Pi_{1u}(2) - {}^1\Pi_{1u}(2)] + {}^3\Delta_{1u}\},$$

where $^3\Pi_{1u}(1)$ and $^1\Pi_{1u}(1)$ have the configuration (2431) while $^3\Pi_{1u}(2)$ and $^1\Pi_{1u}(2)$ share (1342), the two configurations becoming degenerate as $R \rightarrow \infty$. The $^3\Delta_{1u}$ state has the configuration (2332), $^3\Sigma_{1u}^+(1)$ is also (2332) and $^3\Sigma_{1u}^+(2)$ is (1441). As R decreases, interaction between $1_u(1)$, $1_u(2)$, and the other three 1_u states correlating with $^2P_{1/2}$ atoms purges

the $1_u(1)$ state of all but its $^3\Pi_{1u}$ character and $1_u(2)$ becomes predominantly $^1\Pi_{1u}$ by the time the repulsive wall of the potential is reached. The important point in interpreting the present results is that the C state is of singlet character vertically above R_e of the ground state, but acquires equal triplet character as R expands and the spins recouple with the

atomic **L** vectors to give the asymptotic J_A, J_B values.

The single configurations traditionally assigned to the $\Omega=0$ ion-pair states at small R (the region of vertical access from the ground state) are[23] $E(2242;^3\Sigma_{0u}^-)$ and $f(1432;^3\Pi_{0u})$. The electronic structure around the potential minimum of these states (all ≈ 2.7 Å) is best described in the $J_{A^+}M_{A^+}J_{B^-}M_{B^-}$ coupling scheme. The experimental evidence for the lack of mixing of the cation J states around R_e is that the intervals between the T_e values of the $E(^3P_2)$, $\beta(^3P_2)$, and the $G(^3P_1)$, $f(^3P_0)$, and the $G'(^1D_2)$, are similar to the Cl$^+$ term values of 697 cm^{-1} for $^3P_1$, 996 cm^{-1} for $^3P_0$, and 11 652 cm^{-1} for $^1D_2$ (measured relative to $^3P_2$). These states of Cl$^+$ are pure Russell–Saunders states in which the cation spin S remains a good quantum number, with relatively little $^3P_2$–$^1D_2$ mixing compared with I$^+$. The consequence for the present discussion is that the spin multiplicity of the ion-pair states of Cl$_2$ at short bond lengths is retained over the whole range of R. Thus, although the excitation scheme $\beta\ ^3\Sigma_{1g}^-\leftarrow C\ ^1\Pi_{1u}\leftarrow X\ ^1\Sigma_g^+$ appears to involve a singlet-triplet transition at the probe stage, by the time the C state has stretched to ≈ 2.5 Å, it has assumed considerable triplet character.

V. CONCLUSIONS

There is compelling evidence for considerable bond stretching when the repulsive walls of the A, B, and C state potentials are used as resonant intermediate states. In particular, the $C\ ^1\Pi_{1u}$ acts as an efficient gateway to the higher vibrational levels of the $\beta\ ^3\Sigma_{1g}^-$ state and to the $[^2\Pi_{1/2}]_c 4s$; 1_g Rydberg state. At the pump frequencies used in the present experiments, the classical point of transition for the second (probe) step, $\beta\leftarrow C$, occurs around 0.5 Å beyond R_e of the ground state. An essentially diabatic picture of the vibronic motion of Cl$_2$ in the various electronic states in the range 63 000–78 000 cm^{-1} emerges from the overlapping Rydberg and ion-pair spectra presented. This, together with the tendency of the states of Cl$_2$ to adopt either singlet or triplet character at short bond distances, accounts for much of the simplicity of the spectra. Perturbations are sufficiently weak

for well-resolved rotational band contours to be observed for selected vibrational levels. B_ν values were obtained for the E, β, and f ion-pair states and an RKR analysis carried out for each of them.

[1] M. S. N. Al-Kahali, R. J. Donovan, K. P. Lawley, and T. Ridley, Chem. Phys. Lett. **220**, 225 (1994).

[2] R. J. Donovan, K. P. Lawley, Z. Min, T. Ridley, and A. J. Yarwood, Chem. Phys. Lett. **226**, 525 (1994).

[3] M. S. N. Al-Kahali, R. J. Donovan, K. P. Lawley, T. Ridley, and A. J. Yarwood, J. Phys. Chem. **99**, 3978 (1995).

[4] M. S. N. Al-Kahali, R. J. Donovan, K. P. Lawley, Z. Min, and T. Ridley (unpublished).

[5] T. Ishiwata, T. Shinzawa, T. Kusayanagi, and I. Tanaka, J. Chem. Phys. **82**, 1788 (1985).

[6] T. Shinzawa, A. Tokunaga, T. Ishiwata, and I. Tanaka, J. Chem. Phys. **83**, 5407 (1985).

[7] T. Ishiwata, A. Ishiguro, and K. Obi, J. Mol. Spectrosc. **147**, 321 (1991).

[8] J-H. Si, T. Ishiwata, and K. Obi, J. Mol. Spectrosc. **147**, 334 (1991).

[9] T. Ishiwata, Y. Kasai, and K. Obi, J. Chem. Phys. **95**, 60 (1991).

[10] T. Ishiwata, J-H. Si, and K. Obi, J. Chem. Phys. **96**, 5678 (1992).

[11] S. D. Peyerimhoff and R. J. Buenker, Chem. Phys. **57**, 279 (1981).

[12] L. Li, R. J. Lipert, H. Park, W. A. Chupka, and S. D. Colson, J. Chem. Phys. **88**, 4608 (1988).

[13] B. G. Koenders, S. M. Koeckhoven, G. J. Kuik, K. E. Drabe, and C. A. De Lange, J. Chem. Phys. **91**, 6042 (1989).

[14] R. J. Stubbs, T. A. York, and J. Comer, J. Phys. B **18**, 3229 (1985).

[15] D. Maric, J. P. Burrows, R. Miller, and G. K. Moortgat, J. Photochem. Photobiol. A **70**, 205 (1993).

[16] T. Ishiwata, A. Ishiguro, and K. Obi, J. Mol. Spectrosc. **147**, 300 (1991).

[17] M. S. N. Al-Kahali, R. J. Donovan, K. P. Lawley, and T. Ridley, following paper, J. Chem. Phys. **104**, 1833 (1996).

[18] A. M. Cantu, W. H. Parkinson, T. Grisendi and G. Tagliaferri, Phys. Scr. **31**, 579 (1985).

[19] R. P. Tuckett and S. D. Peyerimhoff, Chem. Phys. **83**, 203 (1984).

[20] J. A. Coxon, J. Mol. Spectrosc. **82**, 264 (1980).

[21] J. Strempel and W. Kiefer, J. Chem. Phys. **95**, 2391 (1991).

[22] J. B. Burkholder and E. J. Bair, J. Chem. Phys. **87**, 1859 (1983).

[23] R. S. Mulliken, J. Chem. Phys. **55**, 288 (1971).

[24] M. Sauté and M. Aubert-Frécon, J. Chem. Phys. **77**, 1909 (1986).